Intercalated Organic Redox-active Anions for Enhanced Capacity of Layered Double Hydroxides

Patrick Gerlach, Camille Douard, Insaf Gaalich, Laurence Athouël, Julien Sarmet, Fabrice Leroux, Christine Tavoit-Gueho, Philippe Stevens, Gwenaëlle Toussaint, Thierry Brousse

Intercalated Organic Redox-active Anions for Enhanced Capacity of Layered Double Hydroxides

Patrick Gerlach[1,2], Camille Douard[1,2], Insaf Gaalich[1,2], Julien Sarmet[3], Fabrice Leroux[3], Christine Tavoit-Gueho[3], Philippe Stevens[2,4], Gwenaëlle Toussaint[4], Thierry Brousse[1,2*]

1 Nantes Université, CNRS, Institut des Matériaux de Nantes Jean Rouxel, IMN, 2 rue de la Houssinière BP32229, CEDEX 3, F-44322 Nantes, France

2 Réseau sur le Stockage Electrochimique de l'Energie (RS2E), CNRS FR 3459, 33 rue Saint Leu, CEDEX, F-80039 Amiens, France

3 Université Clermont Auvergne, Institut de Chimie de Clermont-Ferrand (ICCF) UMR n°6296, Clermont Auvergne INP, CNRS, Institut Pascal, F-63000 Clermont-Ferrand, France

4 EDF R&D, Department LME, Avenue des Renardières, CEDEX, F-77818 Moret-sur-Loing,

*corresponding author

Abstract

A Layered Double Hydroxide (LDH) compound LDH ($[Mg_2Al(OH)_6]^+$ x 2 H_2O) intercalated with a redox active organic anion, Anthraquinone-2-sulfonate (AQS), has been envisioned as an electrode material for high power aqueous based battery. The purpose is to use this interlayer redox active molecule for the enhancement of the specific capacity at the LDH composite electrode, which should allow fast charge transfer at the negative electrode for high power storage applications. This is achieved by the reduction of AQS in charge and oxidation in discharge within a redox inactive LDH matrix. The first charge of this new material $[Mg_2Al(OH)_6]^+[AQSO_3]^-$ x 2 H_2O leads to a capacity of 100 mAh g^{-1} at - 0.78 V *vs*. Ag/AgCl (based on the weight of the active material) when operated in aqueous 1 M sodium acetate electrolyte. However, low cycling stability was observed, since a drastic loss in specific capacity occurs after the first charge. This study focuses at elucidating the mechanism behind this phenomenon via in-situ UV/vis experiments. Subsequently, the

dissolution of charged AQS anions into the electrolyte during the first charge of the anode has been identified and quantified. Such understanding of fading mechanism might lead to the design of improved LDH-based electrodes, which utilize redox active anions working in the positive potential range with enhanced cycling ability.

1. Introduction

Layered Double Hydroxides (LDHs), also known as hydrotalcite-like compounds, are a versatile class of 2D intercalation clay compounds described by the general formula: $[M^{2+}_{1-x}M^{3+}_{x}(OH)_2]^{x+}(A^{n-})_{x/n}.yH_2O$, where M^{2+} and M^{3+} are divalent and trivalent metals cations, respectively, and A^{n-} represents an n-valent anion [1,2]. The most popular example showing this characteristic structure is hydrotalcite $Mg_6Al_2(OH)_{16}CO_3 \cdot {}_4H_2O$ [3]. The cation couple (Mg/Al) has been widely studied in this context but other divalent (Zn, Cu, Mn, etc.) and trivalent (Fe, Cr, Co, etc.) cations can be found and are used in LDHs as well [1,2,4–12]. The structure of a single LDH layer is similar to brucite $Mg(OH)_2$, with edge-sharing $M(OH)_6$ octahedra in which the partial substitution of M^{3+} for M^{2+} introduces a net positive charge to the layers balanced by intercalated exchangeable anions (see Figure 1).

By modifying the substitution ratio and/or the intercalated anions, it is possible to obtain a large variety of synthesized phases, which enables a high diversity in physical and chemical properties. Different intercalated organic and inorganic anions enable the design of LDHs for many different applications such as drug delivery [13–16], bio-imaging [17–19], water purification [20–23], catalysis [24–38], sensors [39–44], additives in polymers [45–47], anti-corrosion films [48–51] and ion exchange [52–54].

Furthermore, since the 1990s, there have also been investigations on LDH based electrodes in order to clarify their electrochemical characteristics [55–60]. Specifically, LDHs with the possibility to use electroactive cations within the layers are promising in this field. Several studies have demonstrated the electrochemical behavior of these layers, such as Vialat et al. with the cobalt LDHs Co(II)Co(III)-CO_3 and CoNiAl-CO_3 [61,62]. Thin film electrodes composed of an electroactive LDH matrix deposited on a carbon conductor exhibit specific capacities

ranging from 14 up to 30 mAh g^{-1}. However, changes of the cation oxidation state usually lead to the destabilization of the layers and to their subsequent delamination [63,64].

These efforts have led to many investigations with the aim to use LDH electrodes (with redox active cations, mainly Ni and Co) as energy storage materials in energy storage devices [65–98]. The literature in this regard, however, must be read carefully, since researchers often report on very high values for specific capacitances C in F g^{-1} for single electrodes, which are unfortunately misleading and do not represent the actual charge storage process of the active material [71,73,85,86]. Indeed, classical supercapacitor calculations are mistakenly applied to these electrodes although faradic redox behavior is often clearly observed (non-constant current in CV and plateaus in galvanic charge/ discharge tests) [99].

LDHs have been investigated in various battery-based systems [100–107] e.g. as Li-ion battery electrodes [108,109], in Li-Sulfur batteries [110–112] and so-called anion, halide or double ion batteries [113–116]. A good example for the application of LDHs in batteries was presented by Yang et al. in 2013 [104]. In this study, a ZnAl-LDH carbon nanotube composite was used as an anode material for a Nickel-Zinc-Battery and displayed an improved discharge capacity of 390 mAh g^{-1} (based on the weight of the anode active material) with high cycling stability compared to classical ZnO, but at the expense of the collapsing of the LDH structure upon cycling.

So far, many energy storage systems from the literature use LDHs with redox active cations within the layers. In this work, however, we specifically target the investigation of the redox activity of the anions intercalated in between these layers to enhance fast charge storage capability. This could increase the energy density of advanced energy storage devices using LDH electrodes, while keeping the LDH backbone all over the cycle life of the electrodes. In order to realize this approach, redox active anionic groups can be intercalated during the synthesis, in between the layers of LDHs with non-redox active cations such as MgAl or CaAl to replace inactive anions like CO_3^{2-}, NO_3^-, Cl^-, or OH^- [2]. Mousty et al. studied this concept in 1994 and successfully intercalated m-Nitrobenzene sulfonate and Anthraquinone sulfonates in a ZnCr-LDH matrix [117]. Furthermore, they were able to show the electrochemical activity of single electrodes derived from these materials but with very low amount of electrode material (few µg) with the purpose of designing a pH sensor. Indeed, such strategy has already been pioneered by our team to enhance the capacity (originated from double

layer capacitance) of different types of carbons [118–120]. In addition our team presented a similar approach for the redox activity of riboflavin- and ferrocene based anions in LDH structures in a very recent study [121]. However, besides this work, to the best of our knowledge there is no study of the use of LDHs as matrices for energy storage application. The higher density of LDHs compared to carbons and the one pot synthesis of AQS-intercalated LDHs (instead of multiple steps for functionalized carbons) are two advantages over the use of AQS-grafted carbons.

Specifically, in this work we intercalated the redox active Anthraquinone-2-sulfonate (AQS) between the layers of the redox inactive LDH $[Mg_2Al(OH)_6]^+$ x 2 H_2O to yield the active material $[Mg_2Al(OH)_6]^+[AQSO_3]^-$ x 2 H_2O (MgAlAQS). We decided to use the redox active group of Anthraquinone (AQ), since it displays high specific capacity and a stable redox potential in organic battery applications [122]. The idealized structure of MgAlAQS is shown in Figure 2A.

The desired reduction process of $[AQSO_3]^-$ to $[AQSO_3]^{3-}$ during the charging process is shown in Figure 2B. The theoretical capacity Q_{th} in mAh g^{-1} (based on the mass of the active material) of this reaction was calculated using equation 1

$$Q_{th} = \frac{z \times F}{M \times 3.6} \quad (1)$$

where z is the number of electrons involved in the redox reaction (z = 2), F is the Faraday constant (F = 9.65 x 10^{-4} C mol^{-1}) and M is the molar mass of MgAlAQS (M = 501 g mol^{-1}). For the calculation, 1 mol of $[AQSO_3]^-$ was assumed per mol of $[Mg_2Al(OH)_6]^+$ x 2 H_2O. This results in a theoretical capacity of 107 mAh g^{-1} for MgAlAQS. The reduction potential of Anthraquinone as well as AQS is found to be at -0.68 V *vs*. SHE, which makes MgAlAQS an anode material to be used at the negative electrode of an energy storage device operated in aqueous electrolyte [123].

Therewith, the intercalation of $[AQSO_3]^-$ in MgAlAQS electrodes results in similar capacities compared to Anthraquinone in organic batteries [123–125]. Meanwhile, the capacities of MgAlAQS electrodes are lower than those obtained in LDHs which use the reaction of the metal cations composing the layers [126]. However, in the latter case the LDH structure is

often destroyed, which is not likely to happen for the structure of AQS intercalated in $[Mg_2Al(OH)_6]^+$.

The resulting schematic setup, which was used in this work, is shown in Figure 3 and displays the MgAlAQS composite working electrode combined with a counter electrode (of any kind) submerged in the electrolyte during the charging process. Note that the reference electrode, which was also utilized in all electrochemical experiments, is not drawn. Details about this setup are given in the experimental part.

With this experimental design, the aim of this work is to investigate the redox activity of the $[AQSO_3]^-$ anion, which is intercalated between the layers of $[Mg_2Al(OH)_6]^+$ x 2 H_2O and therewith to prove the concept of our newly designed approach for the enhancement of the specific capacity of LDH electrodes in energy storage applications.

2. Experimental

A layered double hydroxide of the MgAl type was prepared using a coprecipitation method similar to that described by the usual adapted procedure [121]. 100 mL of deionized and decarbonated water was used and the preparation was carried out in a 250mL reactor under a nitrogen atmosphere. Anthraquinone-2-sulfonate was dissolved in this media at 80°C and the pH was adjusted to 10 with 0.1M NaOH solution following the mole ratio between AQS and Al^{3+} cations of $n_{AQS} = 4n_{Al}$. 25 mL of the aqueous metal chlorides solution (0.333 mol/L in $MgCl_2$ and 0.167 mol/L in $AlCl_3$) was added dropwise to the reactor at 80 °C and under magnetic stirring for 3 h. The pH of the reaction mixture was kept constant at 9.5 by adding a 1M NaOH solution. After complete addition of the metal salts, the reaction mixture was left to age at 80°C for 24 hours. The precipitate was then centrifuged and washed three times with hot water. The solid was further dried in an oven for 24 h at 40°C. The X-ray diffraction spectra of the obtained solid are displayed in S1.

X-ray diffraction analyses were performed using a theta−theta PANalytical X'Pert Pro diffractometer equipped with a Cu anticathode (λKα1 = 1.540598 Å, λKα2 = 1.544426 Å) and a X'Celeretor detector. For the phase identification and refinement of the unit cell parameters of the series samples, patterns were recorded in the range of 2−80°/2θ with a step size of 0.325°/min three times.

Scanning electron microscopy (SEM) images were recorded using a JSM-7500F field-emission scanning electron microscope operating at an acceleration voltage of 3 kV and magnifications of ×1K, ×20K, and ×50K or using a Zeiss MERLIN scanning electron microscope with a magnification of ×10K and an acceleration voltage of 20 kV. Samples to be imaged were mounted on conductive carbon adhesive tabs and coated with a gold thin layer.

The composite working electrodes used in this study have been prepared as described in Ref [121] and consisted of 60% active material (LDH, MgAlAQS), 30 % conductive additive carbon black (Super Graphite, Superior Graphite Co.) and 10% binder (PTFE, Sigma Aldrich, 60 % solution in water). The prepared electrodes resulted in an area of 0.5 cm^2 with a thickness of around 100 µm and an average mass loading of 9.2 mg cm^{-2}. They were pressed into a stainless steel current collector in the form of a grid under 500 MPa. For the UV/vis experiments, smaller electrodes with an average area of 0.04 cm^2 and an average mass loading of 18 mg cm^{-2} have been used.

The investigated electrochemical cells were assembled in a 3-electrode beaker type setup, where the working electrode was the LDH composite electrode, the counter electrode was a platinum wire and an Ag/AgCl (3 M NaCl) electrode was used as the reference electrode. All electrodes were submerged into 10 ml of 1 M sodium acetate ($NaCH_3COO$) aqueous electrolyte.

Electrochemical tests were performed using a multichannel potentiostatic-galvanostatic workstation (BioLogic Science Instruments, VMP3, operated under ECLab software) at room temperature. Before all electrochemical experiments, the cells were set to equilibrium by leaving at open circuit for 1 h. Cyclic voltammetry (CV) measurements were recorded between 0 and –1.2 V vs. Ag/AgCl at a scan rate of 1 or 2 mV s^{-1}. Constant current galvanostatic charge/ discharge experiments were performed between 0 to – 1.2 V *vs*. Ag/AgCl (3 M NaCl) with a current of 0.43 A g^{-1} (4 C).

Electrochemical CV tests for UV/vis analysis were performed in the same conditions using a single channel potentiostat-galvanostat (PalmSens, PalmSens 4).

UV/vis analysis was carried out using a UV/Vis/NIR spectrophotometer (PerkinElmer LAMBDA 1050) in transmission mode. The absorption maximum of AQS in the electrolyte

was located at 330 nm, and absorption spectra were measured in the range between 300 – 360 nm.

3. Results and Discussion

The electrochemical behavior of MgAlAQS electrodes in 1 M $NaCH_3COOH$ aqueous electrolyte during cyclic voltammogram (CV) measurements at a scan rate of 2 mV s^{-1} in the potential range from 0 to – 1.2 V *vs*. Ag/AgCl is shown in Figure 4. The evolution between the first and second CV are shown in Figure 4A, since these are of particular interest in this experimental series. The highest current density in this graph is measured for the first reduction of $[AQSO_3]^-$ to $[AQSO_3]^{3-}$ at - 1.03 V *vs*. Ag/AgCl with a value of 2.01 A g^{-1}. The related charge determined for this first reduction process is 99 mAh g^{-1}, which is very close to the theoretical capacity of MgAlAQS of 107 mAh g^{-1} (93 %). The corresponding oxidation peak of the first CV cycle is obtained at -0.48 V *vs*. Ag/AgCl with a significant loss in maximum current density and charge at 1.54 A g^{-1} and 52 mAh g^{-1}. The coulombic efficiency of this first reduction (charge) and oxidation (discharge) couple is close to 50 %. This indicates a large hysteresis phenomenon occurring at the working electrode already in the first cycle. In the second cycle, a further decrease in the charge related to both redox peaks, specifically for the reduction process, is also observed. The related capacities are 48 mAh g^{-1} and 37 mAh g^{-1} for reduction and oxidation processes respectively, with a coulombic efficiency of 72 %.

The loss in capacity with increasing number of cycles is further illustrated in Figure 4B. After 200 cycles, the degradation results in a charge of 7 mAh g^{-1} for the reduction and 3 mAh g^{-1} for the oxidation (42% coulombic efficiency). The shape of the CV curves towards the more negative potentials suggests an increased contribution from the hydrogen evolution reaction (HER) with increasing cycle number, which could explain the drop in coulombic efficiency.

The results shown in Figure 4, present a continuous decrease in capacity, with a pronounced drop on the first cycle. Since nearly all the electroactive AQS molecules in the electrode respond at the first reduction (close to 93% of the theoretical capacity), it suggests that the successive reduction reactions involve AQS molecules which remain electrochemically active, demonstrating that the redox reaction in Fig. 2B is reversible. However, it also appears that a

second electrochemical reaction, the hydrogen evolution reaction progressively increases with the number of cycles, probably due to an electro catalytic activation of the stainless steel current collector. The onset of the HER on stainless steel in alkaline solution has been reported to be around -0.28V *vs.* RHE (i.e. around -0.48V *vs.* Ag/AgCl/KClsat) [127,128].

The rapid degradation of the MgAlAQS electrode in terms of specific capacity for the charge/ discharge process at a current density of 0.43 A g^{-1}, which corresponds to a 4C rate (full charge or discharge of the electrode within 15 min if the full capacity is utilized), is clearly depicted in Figure 5. A specific capacity of 100 mAh g^{-1} is obtained for the first reduction (charge) of the LDH composite electrode, with a potential plateau at - 0.78 V *vs*. Ag/AgCl (Figure 5A), which matches perfectly with the results recorded in the CVs depicted in Figure 4. However, upon the first re-oxidation (discharge), the active material delivers a specific capacity of only 44 mAh g^{-1} (η_c = 44 %) at - 0.6 V *vs*. Ag/AgCl. Therewith, it is obvious that also in the charge/ discharge process of MgAlAQS a pronounced decrease in specific capacity occurred right after the first reduction of the material and indicates again a strong loss of redox active sites in the working electrode. In the second charge, a specific capacity of 46 mAh g^{-1} is measured which is close to the previous discharge capacity. This confirms that the AQS activity lost during the first charge is no longer available for the following cycles. The second discharge delivers 37 mAh g^{-1} (η_c = 80 %) with a loss which is proportionally lower, suggesting that the remaining redox active sites are slightly more stable in the structure of the LDH during cycling.

The further cycling behavior of the MgAlAQS electrodes in 1M $NaCH_3COOH$ in H_2O is shown in Figure 5B for 200 cycles at the same current density (0.43 A g^{-1}, 4 C). After the significant decrease in specific capacity during the first charge, a continuous decrease is measured. After only 20 cycles, the specific capacity of the working electrode is reduced to 21 mAh g^{-1} and further decreases to very low last cycle capacities for charge and discharge processes of 6 and 5 mAh g^{-1} after 200 cycles, respectively. Apart from the first cycle, the coulombic efficiency ranges from 80 to 90%. The values depicted in Figure 5B are shown more detailed in S2.

Both Figure 4 and Figure 5 show a strong loss of the redox capacity in CV and constant current cycling especially in the first reduction. In order to investigate this electrode degradation, the surface of pristine and cycled MgAlAQS composite electrodes have been

observed by SEM to identify possible changes of the electrode, which could have caused a decline in specific capacity. However, the SEM images of pristine and cycled MgAlAQS electrodes in Figure 6A and B do not reveal any degradation during cycling, since no difference in the composite material can be depicted.

This together with the low coulombic efficiencies obtained of the electrodes indicate that the absence of structural electrode film failure, and instead that unwanted side processes during the cycling are most likely responsible for the degradation of the active material. Furthermore, since neither an apparent change of the electrodes nor additional peaks or plateaus in the cycling experiments were observed, a possible explanation is the dissolution of electro-active AQS anions into the electrolyte. To understand this process and to find evidence for such hypothesis, in-situ UV/vis measurements were carried out to identify changes in the electrolyte during cycling.

The dissolution of AQS shown by an UV/vis experiment in an *in-situ* beaker type glass cell with a MgAlAQS working electrode after 40 min of CV at 1 mV s^{-1} (one forward sweep = 20 minutes, 40 min for a full cycle) between 0 V and -1.2 V *vs.* Ag/AgCl (3 M NaCl) and another MgAlAQS electrode in the same setup during 40 min at open circuit potential (OCP) are compared in Figure 7A. The quantity of AQS in the aqueous electrolyte was calculated from the increase in the absorption maximum of anthraquinone at 330 nm. The quantity in % refers to the amount of AQS remaining in the LDH host structure *vs.* the initial amount of AQS present in the WE. In the first 10 minutes, no significant dissolution is observed neither during OCP nor CV measurement. After 10 minutes, once the potential reaches a critical value on the CV experiment, the evolution of the two curves differs significantly. After 40 minutes at OCP no significant amount of AQS was found in the electrolyte (100 % remaining in the electrode), but a strong dissolution was observed after 10 minutes of the CV reduction sweep. At this point, a steep decrease of the AQS in the WE is calculated until a plateau is reached at 25 % after 25 min of CV, i.e. a strong increase of AQS in the electrolyte is observed up to 75 % of the initial amount intercalated in the electrode (Fig. 7A). At the end of the CV, after 40 minutes, the quantity of AQS in the electrode does not change significantly in the last 15 minutes of the experiment (i.e. during the oxidation sweep), and stays at 25 %.

It is therefore clear that during a CV measurement much more AQS is dissolved in the electrolyte in a very short time in comparison to the amount observed during the OCP test. Figure 7B emphasizes this fact, since here even after 19 days at OCP, there is still 95% of residual AQS in the electrode material, which is much more AQS left in the electrode compared to the CV test.

Based on these results, it is obvious that due to the potential changes during the CV experiment, the majority of the redox active AQS is released from the electrode in the time range between the 10^{th} and the 25^{th} minute. To elucidate this process, Figure 8 overlaps the potential at the electrode, the time and the current (I *vs*. t) from 0 V to -1.2 V *vs*. Ag/AgCl at a scan rate of 1 mV s^{-1} with the evolution of the remaining AQS in the working electrode.

The monitored loss of active sites *vs.* the potential at the MgAlAQS based electrode is shown in Figure 8. The two plots highlight that the dissolution of redox active AQS is caused by the reduction of $[AQSO_3]^-$ to $[AQSO_3]^{3-}$ at the potential range between -0.6 V and - 0.9 V *vs*. Ag/AgCl (between minute 8 and 15). The appearance of reduced $[AQSO_3]^{3-}$ in the electrolyte starts within a short delay after the reduction of the $[AQSO_3]^-$ anions at 11 minutes and continues until a plateau is reached at 25 minutes, which corresponds to the end of the reduction sweep. From there, the following oxidation sweep does not lead to an increase in AQS in the electrode. The final amount of residual AQS in the WE amounts to 25 % after only one CV cycle. This means 75 % is dissolved in the electrolyte and no longer accessible for efficient charge storage for the subsequent cycles. It also shows that the remaining 25% reduced AQS that are still in the electrode can be re-oxidized as indicated from the oxidation peak around -0.65 V *vs*. Ag/AgCl. The redox reaction displayed in the unfolded CV of Figure 8, results in a coulombic efficiency of 23 %, which nicely matches the displayed loss in AQS anions after the first reduction. Therefore, it appears that none of the dissolved AQS reacts at the surface of the electrode. In repeated experiments with the same conditions, other values for the remaining percentage of AQS have been obtained (S3). However, in all tests the same trend and the same potential for the release of AQS anions was observed.

The described loss of active sites in the WE is caused by a charge imbalance after the reduction (charging) of the active material. In the discharged state of $[Mg_2Al(OH)_6]^+[AQSO_3]^-$ x 2 H_2O, $[AQSO_3]^-$ anions compensate the positive charge of the $[Mg_2Al(OH)_6]^+$ layers. In the charged electrode, however, this equilibrium is no more valid due to the presence of

$[AQSO_3]^{3-}$. This specie demands three times more positive charge than $[AQSO_3]^-$, which can, however, not be provided by the LDH layers. Therefore, to restore the charge equilibrium, $[AQSO_3]^{3-}$ anions need to leave the LDH structure. In theory, this process should result to the release of 66 % of the initial quantity of AQS anions out of the electrode to yield to the charged LDH active material $[Mg_2Al(OH)_6]^+([AQSO_3]^{3-})_{0.33}$. This means 33 % of AQS is in the LDH electrode after reduction and 66 % is dissolved in the electrolyte. In reality, release percentages between 60 and 90 % have been measured after 1 CV cycle (40 min) in repetitive experiments (S3). This deviation is possibly explainable by the interaction of the WE with acetate anions from the electrolyte, which are present in abundance and which can be exchanged with $[AQSO_3]^{3-}$ upon cycling the electrode. Additionally, during oxidation and the corresponding polarization towards more positive potentials, the re-intercalation of $[AQSO_3]^{3-}$ is statistically unlikely, since vastly more acetate anions are available in the electrolyte for this process. This release of AQS anions out of the electrode into the electrolyte explains the evident decrease in specific capacity measured after the first reduction of the electrode.

This means that, although we demonstrated the redox activity of AQS in the structure of MgAlAQS, the system is by nature not stable during charging and more efforts must be dedicated to the stabilization of the capacity upon cycling, mainly by preventing electroactive molecules to escape from the LDH interlayer space.

4. Conclusion

In this study, we proved the usability of redox active anions intercalated in between LDH layers for energy storage application. In these experiments, the specific capacity of the first reduction/ charge of AQS anions in MgAlAQS was measured at the potential of - 0.78 V *vs*. Ag/AgCl with a total charge capacity of 100 mAh g^{-1}, which is close to the theoretic capacity and therewith highlights the complete electrochemical activity of the anions immobilized in the LDH interlayer spacing.

However, during all electrochemical experiments, insufficient cycling stability of MgAlAQS was observed, which is caused by the dissolution of charged $[AQSO_3]^{3-}$ into the electrolyte

after the first reduction, which has been evidenced by *in-situ* UV/vis experiments. In this process, the charged anion $[AQSO_3]^{3-}$, unlike the discharged $[AQSO_3]^-$, cause a charge imbalance in the LDH structure and therewith is forced out of the interlayers of the LDH working electrode. With the release of $[AQSO_3]^{3-}$ for charge compensation, these active sites are not accessible for charge storage during subsequent cycles. In order to exploit the redox activity of AQS anions, however, this species has to be reduced, which will in any case cause the described intrinsically low cycling stability of the presented active material $[Mg_2Al(OH)_6]^+[AQSO_3]^- \times 2\ H_2O$.

Therefore, it is necessary to search for other intercalated LDHs, with redox active anions, which show less dissolution during charging or ways to prevent the dissolution of the active species into the electrolyte. We will investigate this approach in future studies. Nevertheless, with the findings of this work a vast variety of possible combinations of LDH structure and redox active groups is opened to be investigated for energy storage application.

Acknowledgement: This research was funded by the French Research Agency ANR AAPG2020 “LaDHy”, ANR-20-CE05-0024-01. Labex STORE-EX (ANR-10-LABX-76-01) is also acknowledged for financial support.

References

[1] G.R. Williams, D. O'Hare, Towards understanding, control and application of layered double hydroxide chemistry, J. Mater. Chem. 16 (2006) 3065. https://doi.org/10.1039/b604895a.

[2] A.I. Khan, D. O'Hare, Intercalation chemistry of layered double hydroxides: recent developments and applications, J. Mater. Chem. 12 (2002) 3191–3198. https://doi.org/10.1039/B204076J.

[3] E. Manasse, E. Manasse, Atti Soc. Toscana Sci. Nat., 1915, 24, 92., Atti Soc. Toscana Sci. Nat. 24 (1915) 92.

[4] R. Schöllhorn, B. Otto, Co-operative anion exchange mechanism of layered transition metal hydroxide systems, J. Chem. Soc., Chem. Commun. (1986) 1222–1223. https://doi.org/10.1039/C39860001222.

[5] Z. Gu, J.J. Atherton, Z.P. Xu, Hierarchical layered double hydroxide nanocomposites: structure, synthesis and applications, Chem. Commun. 51 (2015) 3024–3036. https://doi.org/10.1039/C4CC07715F.

[6] M.-Q. Zhao, Q. Zhang, J.-Q. Huang, F. Wei, Hierarchical Nanocomposites Derived from Nanocarbons and Layered Double Hydroxides - Properties, Synthesis, and Applications, Adv. Funct. Mater. 22 (2012) 675–694. https://doi.org/10.1002/adfm.201102222.

[7] L. Wang, C. Li, M. Liu, D.G. Evans, X. Duan, Large continuous, transparent and oriented self-supporting films of layered double hydroxides with tunable chemical composition, Chem. Commun. (2007) 123–125. https://doi.org/10.1039/B613687G.

[8] L. Li, R. Ma, Y. Ebina, K. Fukuda, K. Takada, T. Sasaki, Layer-by-Layer Assembly and Spontaneous Flocculation of Oppositely Charged Oxide and Hydroxide Nanosheets into Inorganic Sandwich Layered Materials, J. Am. Chem. Soc. 129 (2007) 8000–8007. https://doi.org/10.1021/ja0719172.

[9] X. Guo, F. Zhang, D.G. Evans, X. Duan, Layered double hydroxide films: synthesis, properties and applications, Chem. Commun. 46 (2010) 5197. https://doi.org/10.1039/c0cc00313a.

[10] M. Shao, R. Zhang, Z. Li, M. Wei, D.G. Evans, X. Duan, Layered double hydroxides toward electrochemical energy storage and conversion: design, synthesis and applications, Chem. Commun. 51 (2015) 15880–15893. https://doi.org/10.1039/C5CC07296D.

[11] J. Yu, Q. Wang, D. O'Hare, L. Sun, Preparation of two dimensional layered double hydroxide nanosheets and their applications, Chem. Soc. Rev. 46 (2017) 5950–5974. https://doi.org/10.1039/C7CS00318H.

[12] Q. Wang, D. O'Hare, Recent Advances in the Synthesis and Application of Layered Double Hydroxide (LDH) Nanosheets, Chem. Rev. 112 (2012) 4124–4155. https://doi.org/10.1021/cr200434v.

[13] V.K. Ameena Shirin, R. Sankar, A.P. Johnson, H.V. Gangadharappa, K. Pramod, Advanced drug delivery applications of layered double hydroxide, Journal of Controlled Release. 330 (2021) 398–426. https://doi.org/10.1016/j.jconrel.2020.12.041.

[14] S.-J. Ryu, H. Jung, J.-M. Oh, J.-K. Lee, J.-H. Choy, Layered double hydroxide as novel antibacterial drug delivery system, Journal of Physics and Chemistry of Solids. 71 (2010) 685–688. https://doi.org/10.1016/j.jpcs.2009.12.066.

[15] X. Bi, H. Zhang, L. Dou, Layered Double Hydroxide-Based Nanocarriers for Drug Delivery, Pharmaceutics. 6 (2014) 298–332. https://doi.org/10.3390/pharmaceutics6020298.
[16] K. Zhang, Z. Xu, J. Lu, Z. Tang, H. Zhao, D. Good, M. Wei, Potential for Layered Double Hydroxides-Based, Innovative Drug Delivery Systems, IJMS. 15 (2014) 7409–7428. https://doi.org/10.3390/ijms15057409.
[17] L. Yan, M. Zhou, X. Zhang, L. Huang, W. Chen, V.A.L. Roy, W. Zhang, X. Chen, A Novel Type of Aqueous Dispersible Ultrathin-Layered Double Hydroxide Nanosheets for in Vivo Bioimaging and Drug Delivery, ACS Appl. Mater. Interfaces. 9 (2017) 34185–34193. https://doi.org/10.1021/acsami.7b05294.
[18] Jin, Park, Functional Layered Double Hydroxide Nanohybrids for Biomedical Imaging, Nanomaterials. 9 (2019) 1404. https://doi.org/10.3390/nano9101404.
[19] K.N. Andrade, A.M.P. Pérez, G.G.C. Arízaga, Passive and active targeting strategies in hybrid layered double hydroxides nanoparticles for tumor bioimaging and therapy, Applied Clay Science. 181 (2019) 105214. https://doi.org/10.1016/j.clay.2019.105214.
[20] Y. Zhao, S. He, M. Wei, D.G. Evans, X. Duan, Hierarchical films of layered double hydroxides by using a sol–gel process and their high adaptability in water treatment, Chem. Commun. 46 (2010) 3031. https://doi.org/10.1039/b926906a.
[21] M. Sajid, S.M. Sajid Jillani, N. Baig, K. Alhooshani, Layered double hydroxide-modified membranes for water treatment: Recent advances and prospects, Chemosphere. 287 (2022) 132140. https://doi.org/10.1016/j.chemosphere.2021.132140.
[22] B.M.V. da Gama, R. Selvasembian, D.A. Giannakoudakis, K.S. Triantafyllidis, G. McKay, L. Meili, Layered Double Hydroxides as Rising-Star Adsorbents for Water Purification: A Brief Discussion, Molecules. 27 (2022) 4900. https://doi.org/10.3390/molecules27154900.
[23] M. Zubair, M. Daud, G. McKay, F. Shehzad, M.A. Al-Harthi, Recent progress in layered double hydroxides (LDH)-containing hybrids as adsorbents for water remediation, Applied Clay Science. 143 (2017) 279–292. https://doi.org/10.1016/j.clay.2017.04.002.
[24] D. Tang, Y. Han, W. Ji, S. Qiao, X. Zhou, R. Liu, X. Han, H. Huang, Y. Liu, Z. Kang, A high-performance reduced graphene oxide/ZnCo layered double hydroxide electrocatalyst for efficient water oxidation, Dalton Trans. 43 (2014) 15119–15125. https://doi.org/10.1039/C4DT01924E.
[25] X. Long, J. Li, S. Xiao, K. Yan, Z. Wang, H. Chen, S. Yang, A Strongly Coupled Graphene and FeNi Double Hydroxide Hybrid as an Excellent Electrocatalyst for the Oxygen Evolution Reaction, Angew. Chem. (2014) 5.
[26] Z. Lei, Advances in efficient electrocatalysts based on layered double hydroxides and their derivatives, Journal of Energy Chemistry. (2017) 13.
[27] D. Tang, J. Liu, X. Wu, R. Liu, X. Han, Y. Han, H. Huang, Y. Liu, Z. Kang, Carbon Quantum Dot/NiFe Layered Double-Hydroxide Composite as a Highly Efficient Electrocatalyst for Water Oxidation, ACS Appl. Mater. Interfaces. 6 (2014) 7918–7925. https://doi.org/10.1021/am501256x.
[28] C. Tang, H.-S. Wang, H.-F. Wang, Q. Zhang, G.-L. Tian, J.-Q. Nie, F. Wei, Catalysis: Spatially Confined Hybridization of Nanometer-Sized NiFe Hydroxides into Nitrogen-Doped Graphene Frameworks Leading to Superior Oxygen Evolution Reactivity (Adv. Mater. 30/2015), Adv. Mater. 27 (2015) 4524–4524. https://doi.org/10.1002/adma.201570205.

[29] X. Chen, C. Fu, Y. Wang, W. Yang, D.G. Evans, Direct electrochemistry and electrocatalysis based on a film of horseradish peroxidase intercalated into Ni–Al layered double hydroxide nanosheets, Biosensors and Bioelectronics. 24 (2008) 356–361. https://doi.org/10.1016/j.bios.2008.04.007.

[30] X. Zou, A. Goswami, T. Asefa, Efficient Noble Metal-Free (Electro)Catalysis of Water and Alcohol Oxidations by Zinc−Cobalt Layered Double Hydroxide, J. Am. Chem. Soc. (2013) 4.

[31] B. Ballarin, R. Seeber, D. Tonelli, A. Vaccari, Electrocatalytic properties of nickel(II) hydrotalcite-type anionic clay: application to methanol and ethanol oxidation, Journal of Electroanalytical Chemistry. 463 (1999) 123–127. https://doi.org/10.1016/S0022-0728(98)00436-7.

[32] E. Sca, Electrochemical characterisation of Ni/Al Ã/X hydrotalcites and their electrocatalytic behaviour, Electrochimica Acta. (2002) 11.

[33] Y. Li, Engineering of ZnCo-layered double hydroxide nanowalls toward high-efficiency electrochemical water oxidation, Journal of Materials Chemistry A. (2014) 10.

[34] F. Song, Exfoliation of layered double hydroxides for enhanced oxygen evolution catalysis, NATURE COMMUNICATIONS. (2014) 9.

[35] H. Wang, X. Xiang, F. Li, Facile synthesis and novel electrocatalytic performance of nanostructured Ni–Al layered double hydroxide/carbon nanotube composites, J. Mater. Chem. 20 (2010) 3944. https://doi.org/10.1039/b924911g.

[36] Z. Li, Fast electrosynthesis of Fe-containing layered double hydroxide arrays toward highly efficient electrocatalytic oxidation reactions, Chemical Science. (2015) 8.

[37] X. Lei, F. Zhang, L. Yang, X. Guo, Y. Tian, S. Fu, F. Li, D.G. Evans, X. Duan, Highly crystalline activated layered double hydroxides as solid acid-base catalysts, AIChE J. 53 (2007) 932–940. https://doi.org/10.1002/aic.11118.

[38] K. Ebitani, K. Motokura, K. Mori, T. Mizugaki, K. Kaneda, Reconstructed Hydrotalcite as a Highly Active Heterogeneous Base Catalyst for Carbon−Carbon Bond Formations in the Presence of Water, J. Org. Chem. 71 (2006) 5440–5447. https://doi.org/10.1021/jo060345l.

[39] H. Ai, X. Huang, Z. Zhu, J. Liu, Q. Chi, Y. Li, Z. Li, X. Ji, A novel glucose sensor based on monodispersed Ni/Al layered double hydroxide and chitosan, Biosensors and Bioelectronics. 24 (2008) 1048–1052. https://doi.org/10.1016/j.bios.2008.07.039.

[40] H. Fan, Y. Li, D. Wu, H. Ma, K. Mao, D. Fan, B. Du, H. Li, Q. Wei, Electrochemical bisphenol A sensor based on N-doped graphene sheets, Analytica Chimica Acta. 711 (2012) 24–28. https://doi.org/10.1016/j.aca.2011.10.051.

[41] H. Sohrabi, O. Arbabzadeh, M. Falaki, M.R. Majidi, N. Han, Y. Yoon, A. Khataee, Electrochemical layered double hydroxide (LDH)-based biosensors for pesticides detection in food and environment samples: A review of status and prospects, Food and Chemical Toxicology. 164 (2022) 113010. https://doi.org/10.1016/j.fct.2022.113010.

[42] Y. Wang, Z. Wang, Y. Rui, M. Li, Horseradish peroxidase immobilization on carbon nanodots/CoFe layered double hydroxides: Direct electrochemistry and hydrogen peroxide sensing, Biosensors and Bioelectronics. 64 (2015) 57–62. https://doi.org/10.1016/j.bios.2014.08.054.

[43] B. Ballarin, M. Morigi, E. Scavetta, R. Seeber, D. Tonelli, Hydrotalcite-like compounds as ionophores for the development of anion potentiometric sensors, Journal of Electroanalytical Chemistry. 492 (2000) 7–14. https://doi.org/10.1016/S0022-0728(00)00212-6.

[44] C. Mousty, Sensors and biosensors based on clay-modified electrodes?new trends, Applied Clay Science. 27 (2004) 159–177. https://doi.org/10.1016/j.clay.2004.06.005.
[45] Y. Gao, J. Wu, Q. Wang, C.A. Wilkie, D. O'Hare, Flame retardant polymer/layered double hydroxide nanocomposites, J. Mater. Chem. A. 2 (2014) 10996. https://doi.org/10.1039/c4ta01030b.
[46] D.G. Evans, X. Duan, Preparation of layered double hydroxides and their applications as additives in polymers, as precursors to magnetic materials and in biology and medicine, Chem. Commun. (2006) 485–496. https://doi.org/10.1039/B510313B.
[47] A. Illaik, C. Vuillermoz, S. Commereuc, C. Taviot-Guého, V. Verney, F. Leroux, Reactive and functionalized LDH fillers for polymer, Journal of Physics and Chemistry of Solids. 69 (2008) 1362–1366. https://doi.org/10.1016/j.jpcs.2007.10.019.
[48] D. Li, F. Wang, X. Yu, J. Wang, Q. Liu, P. Yang, Y. He, Y. Wang, M. Zhang, Anticorrosion organic coating with layered double hydroxide loaded with corrosion inhibitor of tungstate, Progress in Organic Coatings. 71 (2011) 302–309. https://doi.org/10.1016/j.porgcoat.2011.03.023.
[49] F. Zhang, L. Zhao, H. Chen, S. Xu, D.G. Evans, X. Duan, Corrosion Resistance of Superhydrophobic Layered Double Hydroxide Films on Aluminum, Angew. Chem. 120 (2008) 2500–2503. https://doi.org/10.1002/ange.200704694.
[50] F. Zhang, M. Sun, S. Xu, L. Zhao, B. Zhang, Fabrication of oriented layered double hydroxide films by spin coating and their use in corrosion protection, Chemical Engineering Journal. 141 (2008) 362–367. https://doi.org/10.1016/j.cej.2008.03.016.
[51] S.K. Poznyak, J. Tedim, L.M. Rodrigues, A.N. Salak, M.L. Zheludkevich, L.F.P. Dick, M.G.S. Ferreira, Novel Inorganic Host Layered Double Hydroxides Intercalated with Guest Organic Inhibitors for Anticorrosion Applications, ACS Appl. Mater. Interfaces. 1 (2009) 2353–2362. https://doi.org/10.1021/am900495r.
[52] C. Taviot-Guého, Y. Feng, A. Faour, F. Leroux, Intercalation chemistry in a LDH system: anion exchange process and staging phenomenon investigated by means of time-resolved, in situ X-ray diffraction, Dalton Trans. 39 (2010) 5994. https://doi.org/10.1039/c001678k.
[53] A.V. Radha, P. Vishnu Kamath, C. Shivakumara, Mechanism of the anion exchange reactions of the layered double hydroxides (LDHs) of Ca and Mg with Al, Solid State Sciences. 7 (2005) 1180–1187. https://doi.org/10.1016/j.solidstatesciences.2005.05.004.
[54] L. Lv, P. Sun, Z. Gu, H. Du, X. Pang, X. Tao, R. Xu, L. Xu, Removal of chloride ion from aqueous solution by ZnAl-NO3 layered double hydroxides as anion-exchanger, Journal of Hazardous Materials. 161 (2009) 1444–1449. https://doi.org/10.1016/j.jhazmat.2008.04.114.
[55] J. Qiu, G. Villemure, Anionic clay modified electrodes: electrochemical activity of nickel(II) sites in layered double hydroxide films, Journal of Electroanalytical Chemistry. 395 (1995) 159–166. https://doi.org/10.1016/0022-0728(95)04070-5.
[56] J. Qiu, G. Villemure, Anionic clay modified electrodes: electron transfer mediated by electroactive nickel, cobalt or manganese sites in layered double hydroxide films, Journal of Electroanalytical Chemistry. 428 (1997) 165–172. https://doi.org/10.1016/S0022-0728(96)05070-X.
[57] R. Roto, G. Villemure, Electrochemical impedance spectroscopy of electrodes modified with thin films of MgMnCO3 layered double hydroxides, Electrochimica Acta. 51 (2006) 2539–2546. https://doi.org/10.1016/j.electacta.2005.07.039.

[58] Y. Wang, W. Yang, C. Chen, D.G. Evans, Fabrication and electrochemical characterization of cobalt-based layered double hydroxide nanosheet thin-film electrodes, Journal of Power Sources. 184 (2008) 682–690. https://doi.org/10.1016/j.jpowsour.2008.02.017.

[59] R. Roto, G. Villemure, Mass transport in thin films of [Fe(CN)6]4− exchanged Ni–Al layered double hydroxide monitored with an electrochemical quartz crystal microbalance, Journal of Electroanalytical Chemistry. 588 (2006) 140–146. https://doi.org/10.1016/j.jelechem.2005.12.014.

[60] G. Villemure, A.J. Bard, Part 9. Electrochemical studies of the electroactive fraction of adsorbed species in reduced-charge and preadsorbed clay films, (n.d.) 15.

[61] P. Vialat, C. Mousty, C. Taviot-Gueho, G. Renaudin, H. Martinez, J.-C. Dupin, E. Elkaim, F. Leroux, High-Performing Monometallic Cobalt Layered Double Hydroxide Supercapacitor with Defined Local Structure, Advanced Functional Materials. 24 (2014) 4831–4842. https://doi.org/10.1002/adfm.201400310.

[62] P. Vialat, F. Leroux, C. Taviot-Gueho, G. Villemure, C. Mousty, Insights into the electrochemistry of (CoxNi(1−x))2Al–NO3 Layered Double Hydroxides, Electrochimica Acta. 107 (2013) 599–610. https://doi.org/10.1016/j.electacta.2013.06.033.

[63] E. Duquesne, S. Betelu, A. Seron, I. Ignatiadis, H. Perrot, C. Debiemme-Chouvy, Tuning Redox State and Ionic Transfers of Mg/Fe-Layered Double Hydroxide Nanosheets by Electrochemical and Electrogravimetric Methods, Nanomaterials (Basel). 10 (2020) E1832. https://doi.org/10.3390/nano10091832.

[64] M.J. Young, T. Kiryutina, N.M. Bedford, T.J. Woehl, C.U. Segre, Discovery of Anion Insertion Electrochemistry in Layered Hydroxide Nanomaterials, Sci Rep. 9 (2019) 2462. https://doi.org/10.1038/s41598-019-39052-1.

[65] J. Xu, S. Gai, F. He, N. Niu, P. Gao, Y. Chen, P. Yang, A sandwich-type three-dimensional layered double hydroxide nanosheet array/graphene composite: fabrication and high supercapacitor performance, J. Mater. Chem. A. 2 (2014) 1022–1031. https://doi.org/10.1039/C3TA14048B.

[66] X. Li, J. Shen, W. Sun, X. Hong, R. Wang, X. Zhao, X. Yan, A super-high energy density asymmetric supercapacitor based on 3D core–shell structured NiCo-layered double hydroxide@carbon nanotube and activated polyaniline-derived carbon electrodes with commercial level mass loading, J. Mater. Chem. A. 3 (2015) 13244–13253. https://doi.org/10.1039/C5TA01292A.

[67] D. Yu, B. Wu, J. Ran, L. Ge, L. Wu, H. Wang, T. Xu, An ordered ZIF-8-derived layered double hydroxide hollow nanoparticles-nanoflake array for high efficiency energy storage, J. Mater. Chem. A. 4 (2016) 16953–16960. https://doi.org/10.1039/C6TA07032A.

[68] H. Wang, Q. Gao, J. Hu, Asymmetric capacitor based on superior porous Ni–Zn–Co oxide/hydroxide and carbon electrodes, Journal of Power Sources. 195 (2010) 3017–3024. https://doi.org/10.1016/j.jpowsour.2009.11.059.

[69] X. Li, Z. Yang, W. Qi, Y. Li, Y. Wu, S. Zhou, S. Huang, J. Wei, H. Li, P. Yao, Binder-free Co3O4@NiCoAl-layered double hydroxide core-shell hybrid architectural nanowire arrays with enhanced electrochemical performance, Applied Surface Science. 363 (2016) 381–388. https://doi.org/10.1016/j.apsusc.2015.12.039.

[70] J. Wang, J. You, Z. Li, P. Yang, X. Jing, M. Zhang, Capacitance performance of porous nickel electrode modified with Co/Al hydrotalcite, Journal of Electroanalytical Chemistry. 624 (2008) 241–244. https://doi.org/10.1016/j.jelechem.2008.09.011.

[71] Y. Jiang, Y. Song, Y. Li, W. Tian, Z. Pan, P. Yang, Y. Li, Q. Gu, L. Hu, Charge Transfer in Ultrafine LDH Nanosheets/Graphene Interface with Superior Capacitive Energy Storage Performance, ACS Appl. Mater. Interfaces. 9 (2017) 37645–37654. https://doi.org/10.1021/acsami.7b09373.

[72] K. Ma, J.P. Cheng, F. Liu, X. Zhang, Co-Fe layered double hydroxides nanosheets vertically grown on carbon fiber cloth for electrochemical capacitors, Journal of Alloys and Compounds. 679 (2016) 277–284. https://doi.org/10.1016/j.jallcom.2016.04.059.

[73] J.-J. Zhou, Q. Li, C. Chen, Y.-L. Li, K. Tao, L. Han, Co3O4@CoNi-LDH core/shell nanosheet arrays for high-performance battery-type supercapacitors, Chemical Engineering Journal. 350 (2018) 551–558. https://doi.org/10.1016/j.cej.2018.06.023.

[74] F. Ning, M. Shao, C. Zhang, S. Xu, M. Wei, X. Duan, Co3O4@layered double hydroxide core/shell hierarchical nanowire arrays for enhanced supercapacitance performance, Nano Energy. 7 (2014) 134–142. https://doi.org/10.1016/j.nanoen.2014.05.002.

[75] M. Shao, F. Ning, Y. Zhao, J. Zhao, M. Wei, D.G. Evans, X. Duan, Core−Shell Layered Double Hydroxide Microspheres with Tunable Interior Architecture for Supercapacitors, Chem. Mater. (2012) 6.

[76] X. Wu, L. Jiang, C. Long, T. Wei, Z. Fan, Dual Support System Ensuring Porous Co–Al Hydroxide Nanosheets with Ultrahigh Rate Performance and High Energy Density for Supercapacitors, Adv. Funct. Mater. (2015) 8.

[77] L.-H. Su, X.-G. Zhang, Effect of carbon entrapped in Co–Al double oxides on structural restacking and electrochemical performances, Journal of Power Sources. (2007) 8.

[78] X. Zhang, C.B. Cockreham, E. Yılmaz, G. Li, N. Li, S. Ha, L. Fu, J. Qi, H. Xu, D. Wu, Energetic Cost for Being “Redox-Site-Rich” in Pseudocapacitive Energy Storage with Nickel–Aluminum Layered Double Hydroxide Materials, J. Phys. Chem. Lett. 11 (2020) 3745–3753. https://doi.org/10.1021/acs.jpclett.0c00865.

[79] L. Zhang, X. Zhang, L. Shen, B. Gao, L. Hao, X. Lu, F. Zhang, B. Ding, C. Yuan, Enhanced high-current capacitive behavior of graphene/CoAl-layered double hydroxide composites as electrode material for supercapacitors, Journal of Power Sources. 199 (2012) 395–401. https://doi.org/10.1016/j.jpowsour.2011.10.056.

[80] M. Li, F. Liu, J.P. Cheng, J. Ying, X.B. Zhang, Enhanced performance of nickel–aluminum layered double hydroxide nanosheets / carbon nanotubes composite for supercapacitor and asymmetric capacitor, Journal of Alloys and Compounds. 635 (2015) 225–232. https://doi.org/10.1016/j.jallcom.2015.02.130.

[81] J. Yang, C. Yu, X. Fan, Z. Ling, J. Qiu, Y. Gogotsi, Facile fabrication of MWCNT-doped NiCoAl-layered double hydroxide nanosheets with enhanced electrochemical performances, J. Mater. Chem. A. 1 (2013) 1963–1968. https://doi.org/10.1039/C2TA00832G.

[82] J. Han, Y. Dou, J. Zhao, M. Wei, D.G. Evans, X. Duan, Flexible CoAl LDH@PEDOT Core/Shell Nanoplatelet Array for High-Performance Energy Storage, (2013) 9.

[83] Z. Gao, J. Wang, Z. Li, W. Yang, B. Wang, M. Hou, Y. He, Q. Liu, T. Mann, P. Yang, M. Zhang, L. Liu, Graphene Nanosheet/Ni2+/Al3+ Layered Double-Hydroxide Composite as a Novel Electrode for a Supercapacitor, Chemistry of Materials. (2011) 8.

[84] B. Wang, G.R. Williams, Z. Chang, M. Jiang, J. Liu, X. Lei, X. Sun, Hierarchical NiAl Layered Double Hydroxide/Multiwalled Carbon Nanotube/Nickel Foam Electrodes with Excellent Pseudocapacitive Properties, ACS Appl. Mater. Interfaces. 6 (2014) 16304–16311. https://doi.org/10.1021/am504530e.

[85] H. Liang, J. Lin, H. Jia, S. Chen, J. Qi, J. Cao, T. Lin, W. Fei, J. Feng, Hierarchical NiCo-LDH@NiOOH core-shell heterostructure on carbon fiber cloth as battery-like electrode for supercapacitor, Journal of Power Sources. 378 (2018) 248–254. https://doi.org/10.1016/j.jpowsour.2017.12.046.

[86] J. Zhao, J. Chen, S. Xu, M. Shao, Q. Zhang, F. Wei, J. Ma, M. Wei, D.G. Evans, X. Duan, Hierarchical NiMn Layered Double Hydroxide/Carbon Nanotubes Architecture with Superb Energy Density for Flexible Supercapacitors, Adv. Funct. Mater. (2014) 9.

[87] J. Wang, Y. Song, Z. Li, Q. Liu, J. Zhou, X. Jing, M. Zhang, Z. Jiang, *In Situ* Ni/Al Layered Double Hydroxide and Its Electrochemical Capacitance Performance, Energy Fuels. 24 (2010) 6463–6467. https://doi.org/10.1021/ef101150b.

[88] L. Wang, D. Wang, X.Y. Dong, Z.J. Zhang, X.F. Pei, X.J. Chen, B. Chen, J. Jin, Layered assembly of graphene oxide and Co–Al layered double hydroxide nanosheets as electrode materials for supercapacitors, Chem. Commun. 47 (2011) 3556. https://doi.org/10.1039/c0cc05420h.

[89] J. Zhao, S. Xu, K. Tschulik, R.G. Compton, M. Wei, D. O'Hare, D.G. Evans, X. Duan, Molecular-Scale Hybridization of Clay Monolayers and Conducting Polymer for Thin-Film Supercapacitors, Adv. Funct. Mater. 25 (2015) 2745–2753. https://doi.org/10.1002/adfm.201500408.

[90] R. Ma, X. Liu, J. Liang, Y. Bando, T. Sasaki, Molecular-Scale Heteroassembly of Redoxable Hydroxide Nanosheets and Conductive Graphene into Superlattice Composites for High-Performance Supercapacitors, Adv. Mater. (2014) 6.

[91] H. Chen, L. Hu, M. Chen, Y. Yan, L. Wu, Nickel–Cobalt Layered Double Hydroxide Nanosheets for High-performance Supercapacitor Electrode Materials, Adv. Funct. Mater. (2013) 9.

[92] Y. Gu, Z. Lu, Z. Chang, J. Liu, X. Lei, Y. Li, X. Sun, NiTi layered double hydroxide thin films for advanced pseudocapacitor electrodes, J. Mater. Chem. A. 1 (2013) 10655. https://doi.org/10.1039/c3ta10954b.

[93] V. Gupta, S. Gupta, N. Miura, Potentiostatically deposited nanostructured CoxNi1−x layered double hydroxides as electrode materials for redox-supercapacitors, Journal of Power Sources. 175 (2008) 680–685. https://doi.org/10.1016/j.jpowsour.2007.09.004.

[94] X.-M. Liu, Y.-H. Zhang, X.-G. Zhang, S.-Y. Fu, Studies on Me/Al-layered double hydroxides (Me = Ni and Co) as electrode materials for electrochemical capacitors, Electrochimica Acta. 49 (2004) 3137–3141. https://doi.org/10.1016/j.electacta.2004.02.028.

[95] Z.-A. Hu, Y.-L. Xie, Y.-X. Wang, H.-Y. Wu, Y.-Y. Yang, Z.-Y. Zhang, Synthesis and electrochemical characterization of mesoporous CoxNi1−x layered double hydroxides as electrode materials for supercapacitors, Electrochimica Acta. 54 (2009) 2737–2741. https://doi.org/10.1016/j.electacta.2008.11.035.

[96] A.D. Deshmukh, A.R. Urade, A.P. Nanwani, K.A. Deshmukh, D.R. Peshwe, P. Sivaraman, S.J. Dhoble, B.K. Gupta, Two-Dimensional Double Hydroxide Nanoarchitecture with High Areal and Volumetric Capacitance, ACS Omega. 3 (2018) 7204–7213. https://doi.org/10.1021/acsomega.8b00596.

[97] X. Liu, A. Zhou, T. Pan, Y. Dou, M. Shao, J. Han, M. Wei, Ultrahigh-rate-capability of a layered double hydroxide supercapacitor based on a self-generated electrolyte reservoir, J. Mater. Chem. A. 4 (2016) 8421–8427. https://doi.org/10.1039/C6TA02164F.

[98] A.D. Jagadale, G. Guan, X. Li, X. Du, X. Ma, X. Hao, A. Abudula, Ultrathin nanoflakes of cobalt–manganese layered double hydroxide with high reversibility for asymmetric

supercapacitor, Journal of Power Sources. 306 (2016) 526–534. https://doi.org/10.1016/j.jpowsour.2015.12.097.
[99] T. Brousse, D. Belanger, J.W. Long, To Be or Not To Be Pseudocapacitive?, Journal of The Electrochemical Society. (2015) 6.
[100] W.-K. Hu, D. Noréus, Alpha Nickel Hydroxides as Lightweight Nickel Electrode Materials for Alkaline Rechargeable Cells, Chem. Mater. 15 (2003) 974–978. https://doi.org/10.1021/cm021312z.
[101] J. Yao, Y. Li, Y. Li, Y. Zhu, H. Wang, Enhanced cycling performance of Al-substituted α-nickel hydroxide by coating with β-nickel hydroxide, Journal of Power Sources. 224 (2013) 236–240. https://doi.org/10.1016/j.jpowsour.2012.10.008.
[102] Z. Zhang, Z. Yang, J. Huang, Z. Feng, X. Xie, Enhancement of electrochemical performance with Zn-Al-Bi layered hydrotalcites as anode material for Zn/Ni secondary battery, Electrochimica Acta. 155 (2015) 61–68. https://doi.org/10.1016/j.electacta.2014.12.145.
[103] Y. Liu, Z. Yang, Intercalation of sulfate anions into a Zn–Al layered double hydroxide: their synthesis and application in Zn–Ni secondary batteries, RSC Adv. 6 (2016) 68584–68591. https://doi.org/10.1039/C6RA09096F.
[104] B. Yang, Z. Yang, R. Wang, T. Wang, Layered double hydroxide/carbon nanotubes composite as a high performance anode material for Ni–Zn secondary batteries, Electrochimica Acta. 111 (2013) 581–587. https://doi.org/10.1016/j.electacta.2013.08.052.
[105] M.A. González, R. Trócoli, I. Pavlovic, C. Barriga, F. La Mantia, Layered double hydroxides as a suitable substrate to improve the efficiency of Zn anode in neutral pH Zn-ion batteries, Electrochemistry Communications. 68 (2016) 1–4. https://doi.org/10.1016/j.elecom.2016.04.006.
[106] A. Sumboja, J. Chen, Y. Zong, P.S. Lee, Z. Liu, NiMn layered double hydroxides as efficient electrocatalysts for the oxygen evolution reaction and their application in rechargeable Zn–air batteries, Nanoscale. 9 (2017) 774–780. https://doi.org/10.1039/C6NR08870H.
[107] G.A. Caravaggio, C. Detellier, Z. Wronski, Synthesis, stability and electrochemical properties of NiAl and NiV layered double hydroxides, J. Mater. Chem. 11 (2001) 912–921. https://doi.org/10.1039/b004542j.
[108] W. Yu, N. Deng, K. Cheng, J. Yan, B. Cheng, W. Kang, Advances in preparation methods and mechanism analysis of layered double hydroxide for lithium-ion batteries and lithium-sulfur batteries, Journal of Energy Chemistry. 58 (2021) 472–499. https://doi.org/10.1016/j.jechem.2020.10.031.
[109] L. Shi, Y. Chen, R. He, X. Chen, H. Song, Graphene-wrapped CoNi-layered double hydroxide microspheres as a new anode material for lithium-ion batteries, Phys. Chem. Chem. Phys. 20 (2018) 16437–16443. https://doi.org/10.1039/C8CP01681J.
[110] S. Liu, X. Zhang, S. Wu, X. Chen, X. Yang, W. Yue, J. Lu, W. Zhou, Crepe Cake Structured Layered Double Hydroxide/Sulfur/Graphene as a Positive Electrode Material for Li–S Batteries, ACS Nano. 14 (2020) 8220–8231. https://doi.org/10.1021/acsnano.0c01694.
[111] J. Zhang, H. Hu, Z. Li, X. Wen, Double-Shelled Nanocages with Cobalt Hydroxide Inner Shell and Layered Double Hydroxides Outer Shell as High-Efficiency Polysulfide Mediator for Lithium–Sulfur Batteries, Angew. Chem. (2016) 5.

[112] J. Zhang, Z. Li, Y. Chen, S. Gao, X.W. (David) Lou, Nickel–Iron Layered Double Hydroxide Hollow Polyhedrons as a Superior Sulfur Host for Lithium–Sulfur Batteries, Angew. Chem. 130 (2018) 11110–11114. https://doi.org/10.1002/ange.201805972.
[113] Q. Yin, J. Zhang, J. Luo, J. Han, M. Shao, M. Wei, A new family of rechargeable batteries based on halide ions shuttling, Chemical Engineering Journal. 389 (2020) 124376. https://doi.org/10.1016/j.cej.2020.124376.
[114] Q. Yin, D. Rao, G. Zhang, Y. Zhao, J. Han, K. Lin, L. Zheng, J. Zhang, J. Zhou, M. Wei, CoFe–Cl Layered Double Hydroxide: A New Cathode Material for High-Performance Chloride Ion Batteries, Adv. Funct. Mater. 29 (2019) 1900983. https://doi.org/10.1002/adfm.201900983.
[115] J. Luo, Q. Yin, J. Zhang, S. Zhang, L. Zheng, J. Han, NiMn-Cl Layered Double Hydroxide/Carbon Nanotube Networks for High-Performance Chloride Ion Batteries, (2020) 10.
[116] Q. Yin, J. Luo, J. Zhang, S. Zhang, J. Han, Y. Lin, J. Zhou, L. Zheng, M. Wei, Ultralong-Life Chloride Ion Batteries Achieved by the Synergistic Contribution of Intralayer Metals in Layered Double Hydroxides, Adv. Funct. Mater. 30 (2020) 1907448. https://doi.org/10.1002/adfm.201907448.
[117] C. Mousty, S. Therias, C. Forano, J.-P. Besse, Anion-exchanging clay-modified electrodes: synthetic layered double hydroxides intercalated with electroactive organic anions, Journal of Electroanalytical Chemistry. 374 (1994) 63–69. https://doi.org/10.1016/0022-0728(94)03346-3.
[118] B.D. Assresahegn, T. Brousse, D. Bélanger, Advances on the use of diazonium chemistry for functionalization of materials used in energy storage systems, Carbon. 92 (2015) 362–381. https://doi.org/10.1016/j.carbon.2015.05.030.
[119] T. Brousse, C. Cougnon, D. Bélanger, Grafting of Quinones on Carbons as Active Electrode Materials in Electrochemical Capacitors, J. Braz. Chem. Soc. (2018). https://doi.org/10.21577/0103-5053.20180015.
[120] G. Pognon, T. Brousse, L. Demarconnay, D. Bélanger, Performance and stability of electrochemical capacitor based on anthraquinone modified activated carbon, Journal of Power Sources. 196 (2011) 4117–4122. https://doi.org/10.1016/j.jpowsour.2010.09.097.
[121] J. Sarmet, F. Leroux, C. Taviot-Gueho, P. Gerlach, C. Douard, T. Brousse, G. Toussaint, P. Stevens, Interleaved Electroactive Molecules into LDH Working on Both Electrodes of an Aqueous Battery-Type Device, Molecules. 28 (2023) 1006. https://doi.org/10.3390/molecules28031006.
[122] S. Lee, G. Kwon, K. Ku, K. Yoon, S.-K. Jung, H.-D. Lim, K. Kang, Recent Progress in Organic Electrodes for Li and Na Rechargeable Batteries, Adv. Mater. 30 (2018) 1704682. https://doi.org/10.1002/adma.201704682.
[123] J.M. Gallmetzer, S. Kröll, D. Werner, D. Wielend, M. Irimia-Vladu, E. Portenkirchner, N.S. Sariciftci, T.S. Hofer, Anthraquinone and its derivatives as sustainable materials for electrochemical applications – a joint experimental and theoretical investigation of the redox potential in solution, Phys. Chem. Chem. Phys. 24 (2022) 16207–16219. https://doi.org/10.1039/D2CP01717B.
[124] J. Bitenc, K. Pirnat, T. Bančič, M. Gaberšček, B. Genorio, A. Randon-Vitanova, R. Dominko, Anthraquinone-Based Polymer as Cathode in Rechargeable Magnesium Batteries, ChemSusChem. 8 (2015) 4128–4132. https://doi.org/10.1002/cssc.201500910.
[125] W. Tang, R. Liang, D. Li, Q. Yu, J. Hu, B. Cao, C. Fan, Highly Stable and High Rate-Performance Na-Ion Batteries Using Polyanionic Anthraquinone as the Organic

Cathode, ChemSusChem. 12 (2019) 2181–2185. https://doi.org/10.1002/cssc.201900539.
[126] A.B. Béléké, E. Higuchi, H. Inoue, M. Mizuhata, Durability of nickel–metal hydride (Ni–MH) battery cathode using nickel–aluminum layered double hydroxide/carbon (Ni–Al LDH/C) composite, Journal of Power Sources. 247 (2014) 572–578. https://doi.org/10.1016/j.jpowsour.2013.08.001.
[127] J. Ekspong, T. Wågberg, Stainless Steel as A Bi-Functional Electrocatalyst—A Top-Down Approach, Materials. 12 (2019) 2128. https://doi.org/10.3390/ma12132128.
[128] F. Yu, F. Li, L. Sun, Stainless steel as an efficient electrocatalyst for water oxidation in alkaline solution, International Journal of Hydrogen Energy. 41 (2016) 5230–5233. https://doi.org/10.1016/j.ijhydene.2016.01.108.
[129] S.J. Mills, A.G. Christy, J.-M.R. Génin, T. Kameda, F. Colombo, Nomenclature of the hydrotalcite supergroup: natural layered double hydroxides, Mineral. Mag. 76 (2012) 1289–1336. https://doi.org/10.1180/minmag.2012.076.5.10.

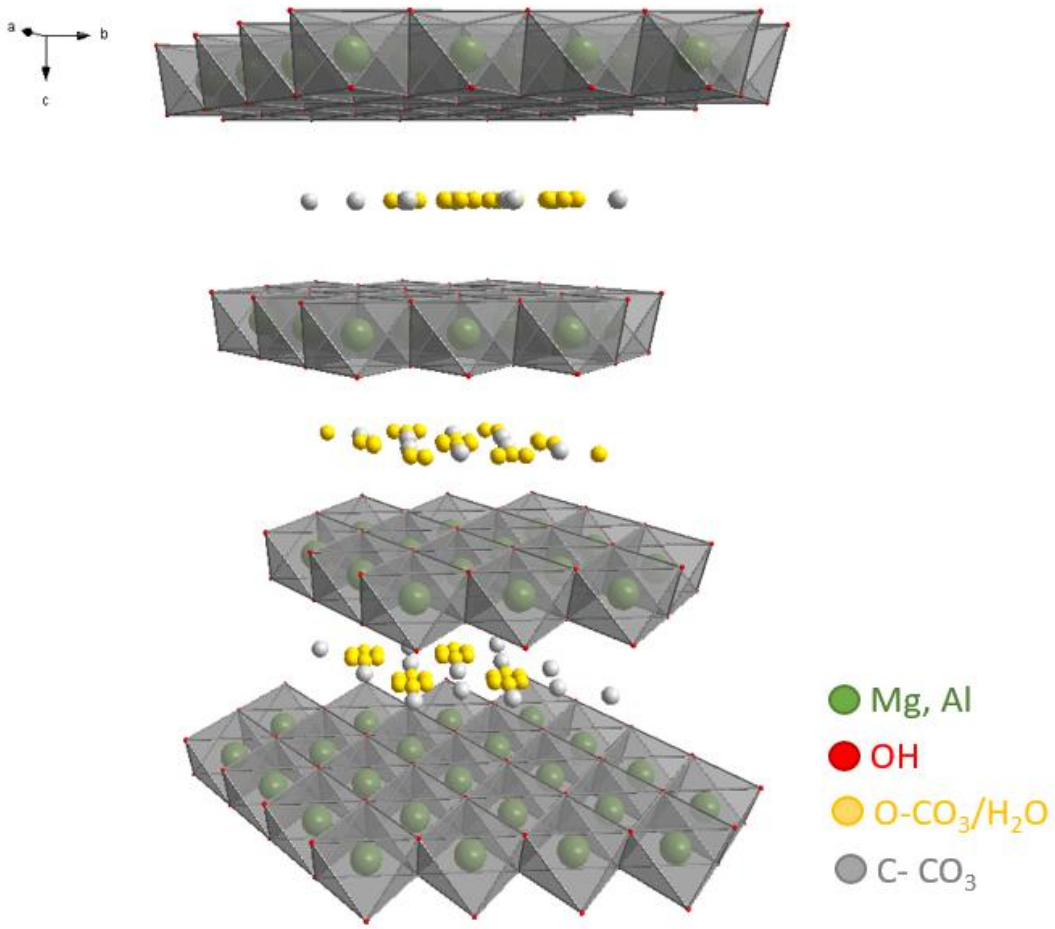

Figure 1 : Atomic structure of Hydrotalcite mineral $Mg_6Al_2(OH)_{16}[CO_3]$ x $4H_2O$ as representative of layered double hydroxide family [129]

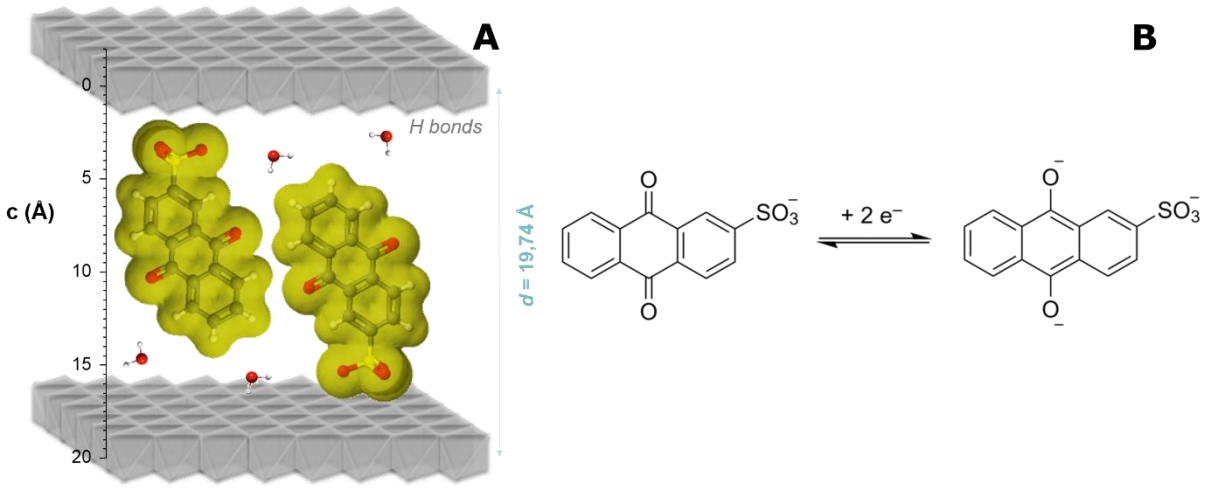

Figure 2: A) Schematic structure LDHs with inserted redox active moieties example AQS, B) Exploited redox reaction of AQS

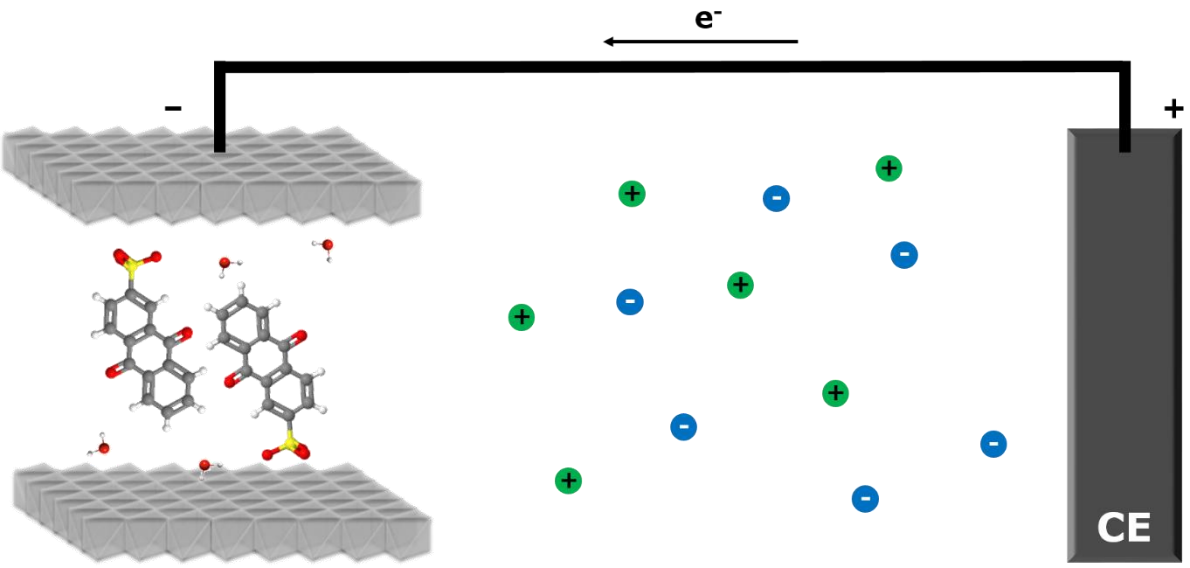

Figure 3 : Concept of MgAlAQS electrode in electrochemical energy storage cell

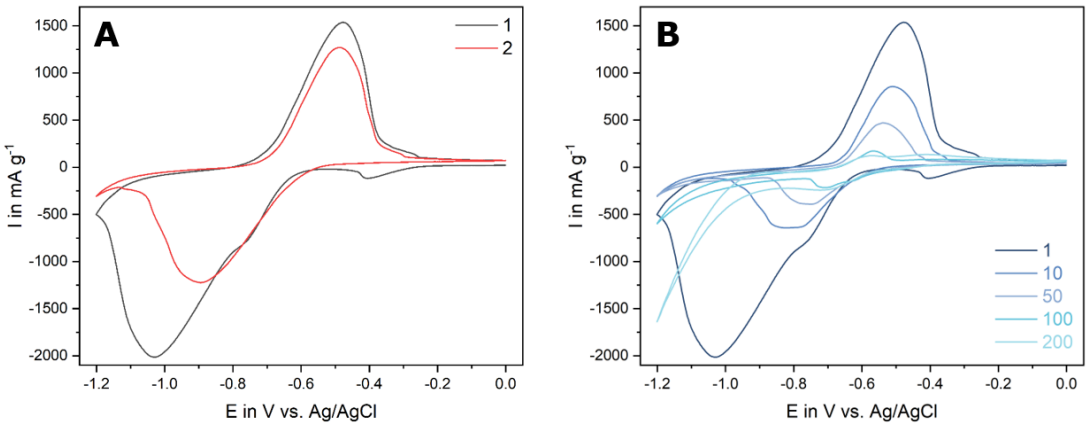

Figure 4 : CVs of MgAlAQS electrodes from 0 to – 1.2 V *vs*. Ag/AgCl at 2 mV s^{-1} in 1 M $NaCH_3COOH$ in H_2O at the cycles 1, 2, 10, 50, 100 and 200.

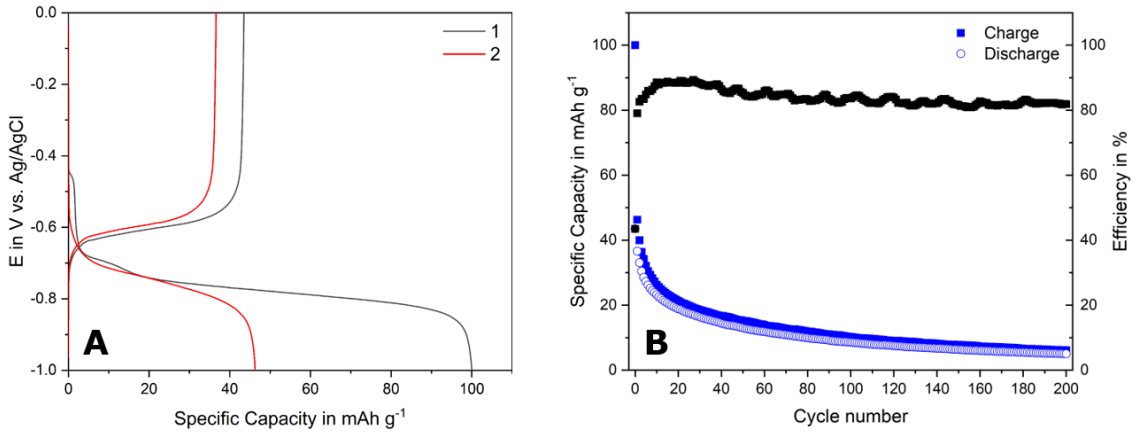

Figure 5 : A) Charge/ discharge profile of MgAlAQS electrodes for the first and second cycle and B) cycling stability at 0.43 A g^{-1}/ 4C in 1 M $NaCH_3COOH$ aqueous electrolyte for 200 cycles

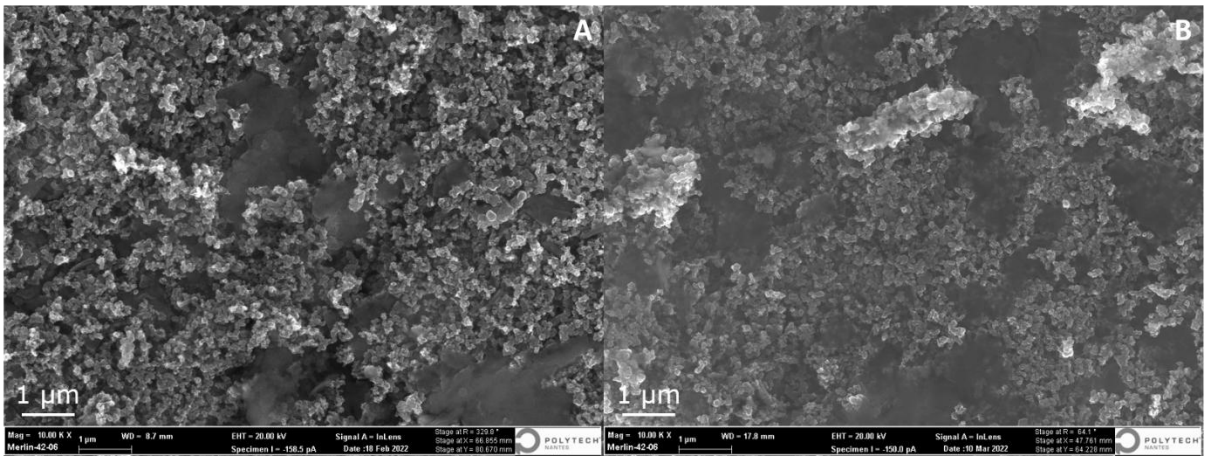

Figure 6 : MgAlAQS electrodes A) pristine and B) after 200 cycles of charge/ discharge in 1 M $NaCH_3COOH$ in H_2O with a magnification of x 10 k, the scale at the bottom left corner is 1 µm

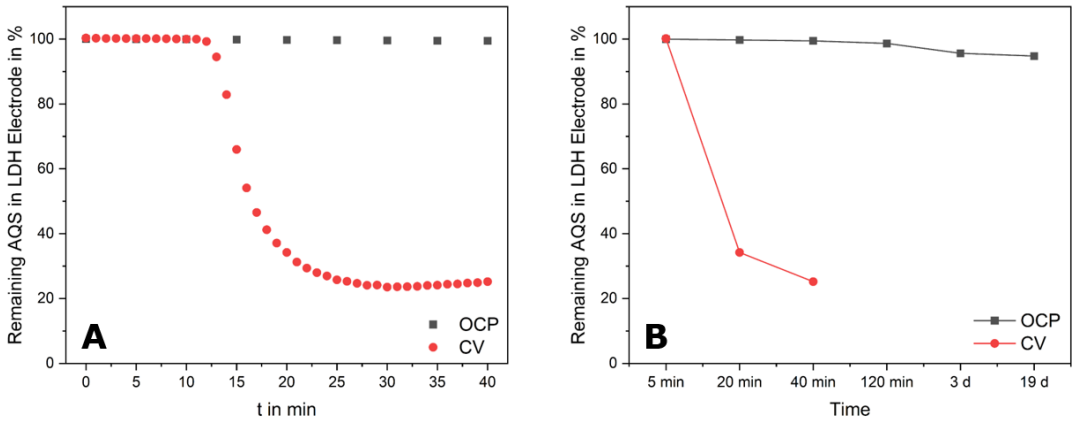

Figure 7: A) In-situ UV-vis measurements of MgAlAQS electrodes in cuvette, B) UV-vis comparison of MgAlAQS electrode in-situ after 19 days of OCP and 40 min CV

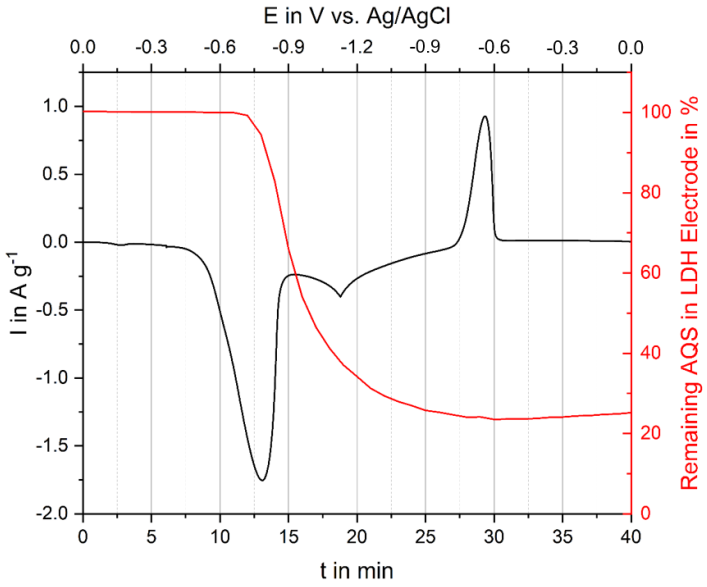

Figure 8 : Loss of AQS in MgAlAQS electrodes at 1 mV s^{-1} overlaid with unfolded CV current I *vs.* time t